Plasmon Resonance of Isolated Gold Hollow Nanoparticles and Nanoparticle Pairs: Insights from Electronic Structure Calculations

ARTICLE *in* THE JOURNAL OF PHYSICAL CHEMISTRY C · JANUARY 2012

Impact Factor: 4.77 · DOI: 10.1021/jp2094092

3 AUTHORS:

Huili Ma
Tsinghua University
7 PUBLICATIONS **37** CITATIONS
SEE PROFILE

Fang Gao
Chinese Academy of Sciences
19 PUBLICATIONS **231** CITATIONS
SEE PROFILE

WanZhen Liang
Xiamen University
76 PUBLICATIONS **2,543** CITATIONS
SEE PROFILE

THE JOURNAL OF PHYSICAL CHEMISTRY C

ARTICLE

pubs.acs.org/JPCC

Plasmon Resonance of Isolated Gold Hollow Nanoparticles and Nanoparticle Pairs: Insights from Electronic Structure Calculations

Huili Ma,[†] Fang Gao,[‡] and WanZhen Liang*[,†]

[†]Hefei National Laboratory for Physical Science at Microscale, and Department of Chemical Physics, University of Science and Technology of China, Hefei 230026, China

[‡]Institute of Intelligent Machines, Chinese Academy of Sciences, Hefei 230031, China

ABSTRACT: Because the feature sizes of noble metal nanoparticles (NPs) are smaller than a few of nanometers, simulations including quantum effects and atomistic details are inevitable. In this work, we report a detailed electronic structure study on the plasmon resonance of isolated gold hollow nanoparticles (NPs) and NP pairs. The long-range-corrected (LRC) density functional theory (DFT) has been employed. We find that the plasmon resonance of small-size gold NPs is very sensitive to NP sizes and interparticle distances. When the NP's size changes from Au32 to $Au17^-$, the high-energy absorption maximum blue shifts 50 nm and when the interparticle distance of $Au17^-$ NP pairs changes from 1.15 to 0.83 nm, the corresponding blue shift is ∼40 nm. The spectral line width becomes narrower as the NP size increases and the interparticle distance reduces. The insight of how the plasmon-resonance peaks of a NP pair are formed and how they are sensitive to the interparticle separation is revealed by the plots of transition densities and frontier molecular orbitals (MOs) as a function of the interparticle distances. As the two NPs approach near touching contact, they are strongly coupled and a bond-forming step takes place, which is verified by the significant overlap between the unoccupied MOs. The strong coupling between the wave functions results in the electrons to redistribute. As a result, we observe that a large number of electrons are localized in the gap and the nearest neighboring atoms of a closely spaced NP pair. The localized electrons enhance the electromagnetic field in the gap of the NP pair, leading to a pronounced red shift and increasing polarizability for the plasmon-resonance peaks, and many new absorption peaks appeared in low-energy range.

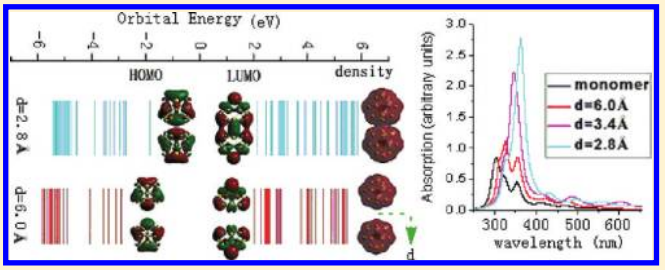

I. INTRODUCTION

The noble metal NPs (NPs) have received considerable attention because of their intense surface plasmon resonance and the ability to tune it by changing the size, shape, composition, and dielectric environment of nanostructures. The surface plasmon resonance is formed by the resonant interaction between photon and collective electron charge oscillations in metallic NPs,[1] which not only makes NPs possess the brilliant optical properties, but also offers a strongly enhanced near field to enhance spectroscopic signals of the adsorbed molecules.[2−7] The noble metal NPs exhibit a strong absorption band in the ultraviolet−visible light region that is absent in the bulk metal and is originated from the collective electron charge oscillations. For example, there is a strong absorption band at ∼520 nm for gold NPs with the diameter 22 nm,[8,9] whereas the resonance is at ∼440 nm for silver spheres, and the line width is narrower. The quasi-static regime holds when the diameter is in the range of approximately 10 to 50 nm, and the plasmon resonance is nearly independent of the particle size but highly sensitive to the shape of the particle and its embedded media.[6,8,10−13] Therefore, a detailed correspondence between the NP structure and its optical response is essential.

The modeling and simulation of the optical response of nanostructures provide a detailed, quantitative understanding of these systems, allowing a close interplay of theory and experiment. Early in the 20th century, it was based on analytical solutions of Maxwell's equations to address light scattering by NPs of simple geometries, such as spheres and ellipsoids. For spheres, the solutions are known as Mie resonances.[14] As the structural complexity of NPs increases, many numerical methods, such as the most commonly used finite difference time domain method,[15] the discrete dipole approximation,[16,17] the multiple multipole method,[18] multiple scattering techniques, transfer matrix approaches[19] and finite-element method,[20] and so on, have been employed to describe the surface plasmon modes of a variety of structures, including slabs, cylinders, cubes, edges, hemispheres, coupled spheres, and NP arrays. These methods have proven to be immensely useful for interpreting a wide range of nanoscience experiments and providing the capability to describe optical properties of particles up to several hundred nanometers in dimension, with arbitrary particle structures and complex dielectric environments taken into consideration. An overview about these analytical and numerical methods

Received: September 29, 2011
Revised: December 15, 2011
Published: December 16, 2011

dx.doi.org/10.1021/jp2094092 | J. Phys. Chem. C 2012, 116, 1755–1763

for the description of electromagnetic properties of silver and gold NPs has recently been provided by Schatz's group.[21] However, as the size of metal particles decreases to the Bohr radius of an exciton, the electronic motion becomes confined and the confinement of the charge carrier discretizes the electronic energy band. As a result, the noble-metal NPs with the diameter <10 nm exhibit molecular-like electronic and optical properties that deviate significantly from their bulk counterparts.[22] Their characteristic plasmon bands are replaced by discrete electronic transitions, which lead to a significant broadening of the plasmon-resonance peak. These small-size NPs are less well understood because the above classical methods fail to resolve their responses to the light, but an inevitable quantum mechanical description including full atomistic details is still challenged.

To reveal the inherent optical response of metal NPs, it is necessary to study single particles. However, NPs can assemble to form aggregates. Multimers of NPs are interesting chemical objects.[23,24] In NP assemblies, their individual plasmons couple together. It is found that the near-field around single NP can be strongly enhanced, for example, the near-field in the gaps between NPs can be enhanced by several additional orders of magnitude due to the interaction between the particles. NP dimer serves as a simple prototypical model system to study the important physical factors underlying the electromagnetic field enhancements. Their plasmonic properties have recently been investigated by a variety of theoretical methods,[24−41] such as the discrete dipole approximation model[26] and the plasmon hybridization model.[30−32] Most of the existing theoretical studies employed either classical electromagnetic interaction or the simplified plasmon hybridization or dipole−dipole coupling models. Those classical approaches provide a simple way to understand the plasmon coupling and are particularly well-suited for weakly coupled nanostructures. However, in strongly coupled or closely spaced NPs, the plasmon of individual particles can be significantly distorted due to the intermolecular polarization effect and exchange electron interaction. The optimal electron distribution in closely spaced NPs can be considerably different from that in weakly coupled NPs. As a result, the simple plasmon hybridization model or dipole−dipole coupling model fail, and a quantum-mechanical treatment to the supermolecular system will be needed.

In this work, we seek an understanding of the plasmon resonance of small-size isolated NPs and coupled NP dimers from an electronic structure calculation. Small-size Au NPs have been widely employed in materials science, catalysis, and biomedicine due to their unique physical and chemical properties. It was found that the most active catalysts were small Au NPs approximately 2 nm in diameter[42] and that the biological applications are also influenced by the size of NPs. For example, biological portals as the nuclear pore complex would only allow a maximal size of 8 nm for a substance to cross passively the nuclear membrane.[43] It is therefore both theoretically and practically important to perform a detailed study on the origin of their unique properties from an electronic structure calculation. We check how the size and interparticle distance of NPs dictate the frequency of the plasmon resonance. The absorption spectra of NPs with different sizes and the NP pairs with different interparticle distances will be calculated with time-dependent density functional theory (TDDFT). Small-size gold clusters, the anion $Au17^-$ and neutral Au32, will be used as our representative systems. The reason why we perform calculations on these two systems is that they both have similar type hollow cage structures,

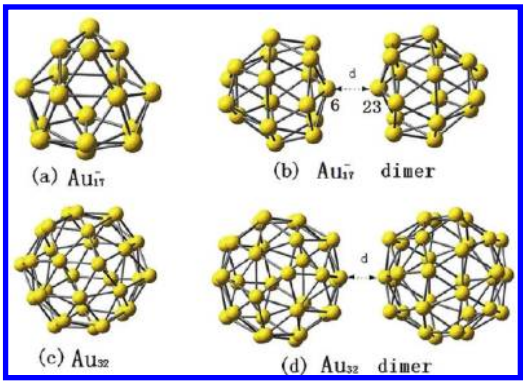

Figure 1. Geometrical structures of $Au17^-$, Au32 NPs, and their dimers. *d* denotes the tip-to-tip distance between neighbor atoms.

that the quantum-size effect and the atomistic detail should be significant for NPs with this feature size, and that it is computationally feasible to perform a many-body electronic-structure calculation on the systems in our local machines. Through the evaluation of absorption spectra, we reveal the effect of NP sizes on the plasmon excitation. Then, from the analysis of the electron transitions between molecular orbitals (MOs), the density matrices, and frontier MOs as a function of the interparticle distances, we give the physical consensus of how the plasmon-resonance peaks are formed in a coupled NP pair and how they are sensitive to the interparticle separation. The spectral alteration of an NP pair with the interparticle distances and NP sizes will be explained by the alteration of the hybridization strength of MOs between the individual NPs. By comparing the exciton interactions calculated by TDDFT and Frenkel exciton model, we reveal the insight of the plasmon resonance in closely spaced NPs.

The structure of this article is arranged as follows: In Section II, we briefly review the computational methods used for the calculation of absorption spectra of $Au17^-$ and Au32 clusters. Section III displays the calculated results and discussions. The concluding remarks are given in Section IV.

II. COMPUTATIONAL DETAILS

The geometries of small and medium-size gold clusters have been determined by experiments and theories in recent years. Small anionic clusters have 2D structures,[44,45] whereas large clusters have been proven to exhibit hollow cage structures.[46−52] Here we choose the anion $Au17^-$[46,47] and neutral Au32[49,52] NPs (shown in Figure 1) as our representative systems. Their structures are taken from the previous works[44,46,52] and are optimized at PBE/lanl2dz theoretical level with Gaussian 03 software package.[53] The anion $Au17^-$ possesses C_{2v} symmetry, and its average diameter is 0.62 nm. The lowest-energy structure of the neutral cluster Au32 has icosahedral (I_h) symmetry, whose average diameter is ∼0.83 nm. The face-to-face orientation with D_{2h} symmetry is adopted for $Au17^-$ dimer, whereas for the Au32 dimer, we set the hexagon rings to face each other with D_{3h} symmetry retained. The dimers should be the most stable structures due to the highest geometry symmetry with separations of the center of mass fixed.

TDDFT has been confirmed to provide efficient descriptions to small gold anionic clusters compared with experimental measurement.[54] However, TDDFT with conventional exchange-correlation (xc) functional has been found to give a poor description

dx.doi.org/10.1021/jp2094092 |J. Phys. Chem. C 2012, 116, 1755–1763

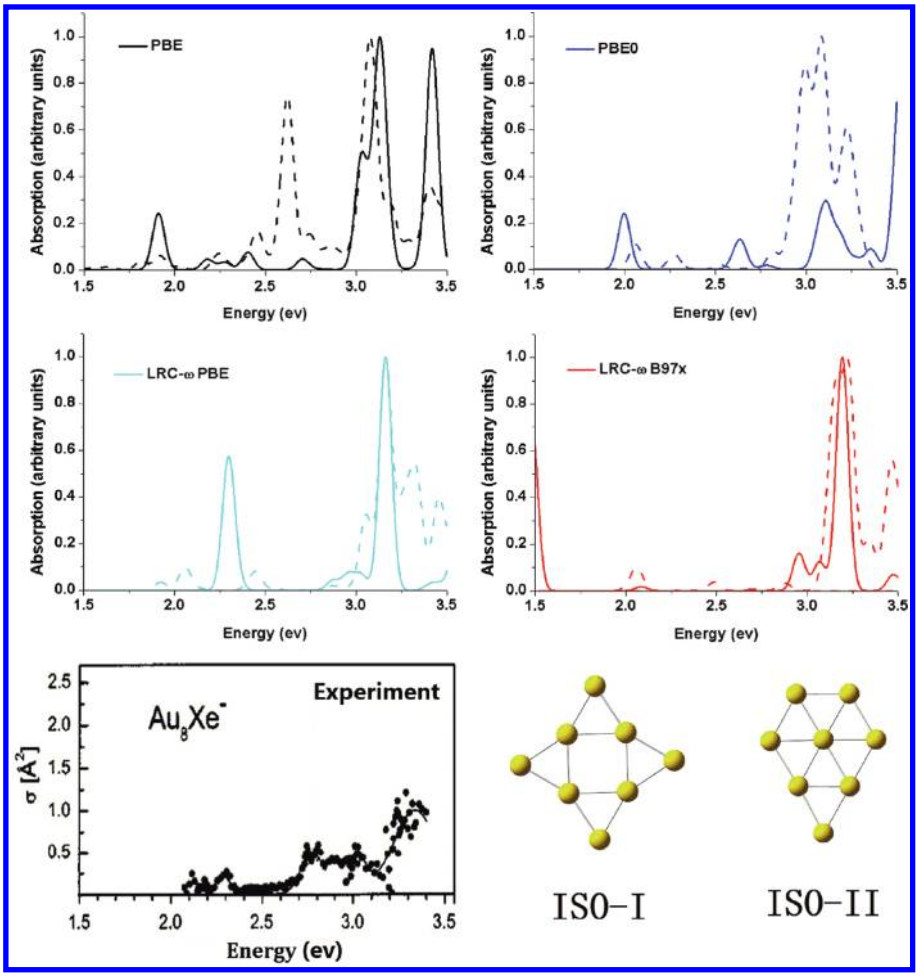

Figure 2. Absorption spectra of Au nanoparticle $Au8^-$ calculated by TDDFT with different xc functionals. The results of isomer I and II are shown with solid and dashed lines, respectively. The spectra were fitted using Gaussian wavelength broadening of δ = 0.08 eV.

on the large delocalization excitation and long-range charge transfer excitation due to the nonlocality and incorrect asymptotic behavior for the xc potential. To solve the problem, an alternative choice is to improve the xc functionals by incorporating 100% Hartree−Fock exchange at the long-range, whereas in the short-range the form of traditional generalized gradient approximation (GGA) or hybrid functionals is adopted. This is the so-called long-range-corrected DFT (LRC-DFT) functionals.[55,56] In this work, we will check the effect of DFT xc functionals on the optical properties of gold NPs and their dimers. Four different DFT functionals will be used in this study: the GGA functional PBE,[57] which has been shown to describe the ground-state properties of gold clusters very well;[44,46,52] the hybrid xc functional PBE0 (C_{HF} = 0.27)[58] and two LRC-DFT functionals, including LRC-ωB97x (C_{HF} = 0.157706, ω = 0.3 $Bohr^{-1}$)[59] and LRC-ωPBE (C_{HF} = 0.0, ω = 0.3 $Bohr^{-1}$).[56] All TDDFT calculations are carried out within the Q-chem software package.[60]

III. RESULTS AND DISCUSSION

A. Effect of xc Functionals. Small gold cluster $Au8^-$ is used as a test molecule to check the effect of xc functionals on the optical properties of gold NPs. $Au8^-$ NP has two isomer structures as shown in Figure 2. The experimental results show that the absorption bands appear around 2.3 and 2.8 to 3.5 eV.[54] The theoretical studies demonstrate that both the DFT xc functionals and geometrical conformations have a significant influence on the spectra. Taking the average of the calculated results of the two isomers and then comparing it with the experimental measurements, we find that both the hybrid xc functional and LRC-DFT functionals show better performance than GGA functional PBE. Here the absorption spectra of $Au8^-$ cluster are fitted by Gaussian line shape with a full width of half-maximum (fwhm) of 0.08 eV to compare with the experimental results.

The effect of DFT xc functionals on the optical spectra of larger Au32 cluster has also been investigated. (See Figure 3.) PBE functional yields three major absorption bands centered at 497, 610, and 750 nm, respectively. The two high-energy bands possess similar oscillator strengths, which are considerably weaker than the bands centered at ~350 nm yielded by TD-LRC-DFT. TD-LRC-DFT correctly yields the apparent plasmonic characteristics of Au NPs and places most of the absorption intensity near the absorption maximum. The absorption maxima centered at 337 and 356 are yielded by LRC-ωB97x and LRC-ωPBE, respectively. PBE0 yields a high-energy absorption maximum of 400 nm. Compared with the result of PBE0, it is clear that LRC-DFT functionals overestimate the excitation energies, which has been verified by our previous work.[61] However, LRC-DFT usually can give a better description on both the energy-level spacing and the order of excited states as well as

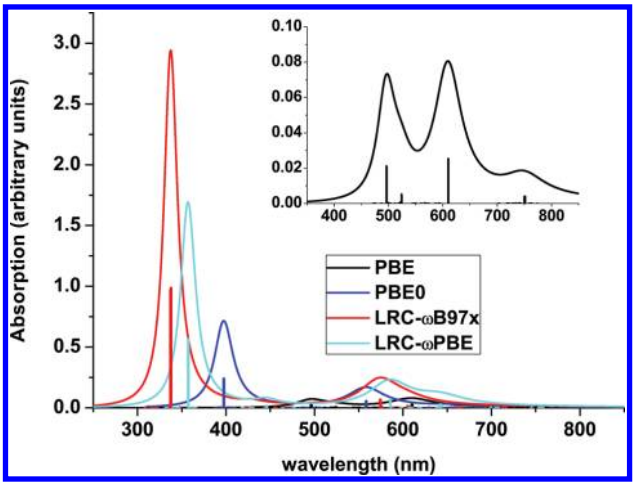

Figure 3. Absorption spectra of Au32 calculated by TDDFT with the different xc functionals. The spectra were fitted with Lorentz energy broadening of δ = 0.2 eV.

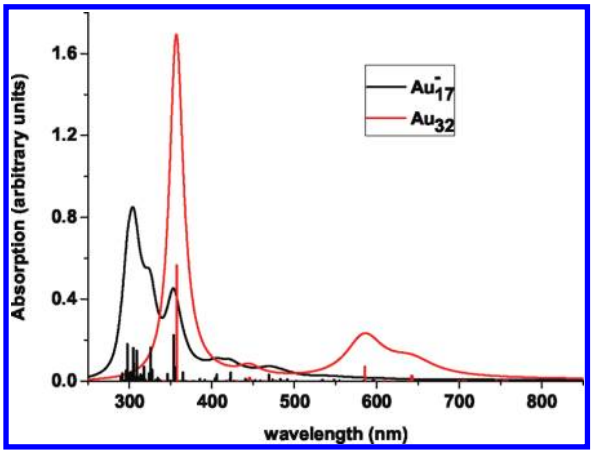

Figure 4. Absorption spectra of $Au17^-$ (solid black line) and Au32 (solid red line) calculated by TD-LRC-ωPBE. The vertical bar denotes oscillator strengths of the corresponding excited states. The spectra were fitted with Lorentz energy broadening of δ = 0.2 eV.

intermolecular CT states than the conventional functionals. Therefore, in the later calculations of isolated NPs and NP pairs, LRC-ωPBE is adopted.

B. Isolated NPs. The absorption spectra of NPs with different sizes are shown in Figure 4. The high-energy absorption maximum included in each monomer spectrum evolves with the cluster sizes. The absorption maximum blue shifts from 357 to 305 nm as the diameter of the gold hollow decreases, in agreement with the experimentally observed bands shift trends.[30−32] The broad absorption bands between 297.78 and 353.80 nm in the absorption spectrum of $Au17^-$ anion mainly consist of six bright singlet excited states (BSESs), which are shown in Table 1. The excited states with very small oscillator strengthes (far less than 0.1), considered as optical dark states, are not included in Table 1. There is an excitation energy difference of 0.66 eV between the first and last bright excited states (39th and 87th excited states), which have similar oscillator strength. Therefore, the expected spectral line width of plasmon excitations should be "wide". Unlike $Au17^-$, the strongest absorption band of Au32 has a narrower linewidth, which is formed by three nearly degenerate BSESs (Table 2). The narrower and stronger high-energy absorption band of Au32

Table 1. Calculated BSESs Composed of the Plasmon-Resonance Band of $Au17^-$[a]

BSES	E (eV)	f	λ (nm)	orbital contributions (amplitude)
S_{39}	3.5067	0.2231	353.8056	H − 5 → L + 1 (0.3900)
				H − 4 → L + 2 (0.4133)
				H − 3 → L + 3 (−0.3166)
				H − 2 → L + 7 (−0.4338)
				H − 1 → L + 5 (−0.2542)
S_{52}	3.8098	0.1629	325.6576	H − 18 → L (0.3250)
				H − 8 → L + 1 (−0.3616)
				H − 6 → L + 2 (0.2867)
				H − 5 → L + 2 (0.2612)
				H → L + 8 (0.5293)
S_{66}	4.0171	0.1477	308.8522	H − 24 → L (0.2515)
				H − 12 → L + 1 (−0.4390)
				H − 8 → L + 2 (0.3992)
				H − 5 → L + 1 (−0.2173)
S_{72}	4.0596	0.0848	305.6188	H − 21 → L (0.2525)
				H − 17 → L (−0.2920)
				H − 10 → L (−0.2573)
				H − 8 → L + 2 (0.6024)
				H − 6 → L + 5 (0.2616)
S_{75}	4.0704	0.1603	304.8079	H − 18 → L (0.3636)
				H − 14 → L (0.2933)
				H − 11 → L + 1 (−0.2421)
				H − 7 → L + 3 (0.3225)
				H → L + 8 (−0.3058)
S_{87}	4.1665	0.1799	297.7776	H − 15 → L + 3 (−0.2656)
				H − 14 → L (−0.4138)
				H − 13 → L + 2 (0.3999)
				H − 10 → L + 3 (0.3222)
				H − 6 → L + 2 (0.2393)

[a] E, f, and λ represent excited energy, oscillator strength, and wavelength, respectively.

Table 2. Calculated BSESs Composed of the Plasmon-Resonance Band of Au32

state	E (eV)	f	λ (nm)	orbital contributions (amplitude)
S_{77}	3.4723	0.5641	357.3107	H − 12 → L + 1 (0.2563)
				H − 6 → L + 5 (−0.2456)
				H − 5 → L + 4 (0.3688)
				H − 5 → L + 8 (−0.2791)
				H − 4 → L + 6 (−0.2688)
S_{78}	3.4726	0.5636	357.2799	H − 14 → L + 1 (−0.2256)
				H − 12 → L (0.2385)
				H − 11 → L + 2 (0.2880)
				H − 6 → L + 4 (−0.2318)
				H − 6 → L + 6 (−0.2583)
				H − 4 → L + 7 (0.4221)
S_{79}	3.4728	0.5623	357.2593	H − 13 → L + 1 (−0.2349)
				H − 6 → L + 5 (−0.3712)
				H − 5 → L + 8 (0.2830)
				H − 4 → L + 6 (0.2852)

dx.doi.org/10.1021/jp2094092 |J. Phys. Chem. C 2012, 116, 1755–1763

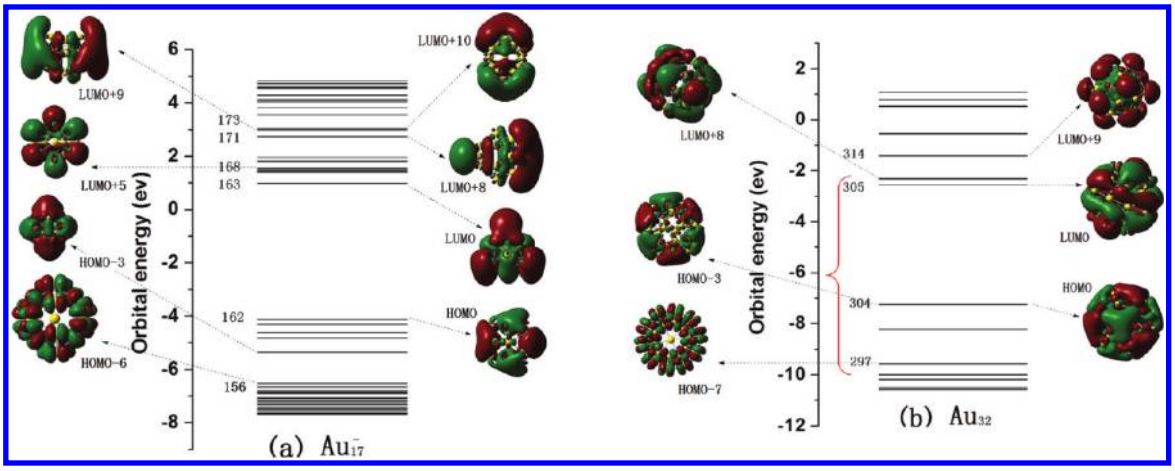

Figure 5. Diagram of MO energy levels and the spatial electron distribution of frontier MOs of $Au17^-$ (a) and Au32 (b).

exhibits more appreciable characteristic of plasmon resonance than that of $Au17^-$. Other two weak bands centered at 585.60 and 641.80 nm are well-separated from the plasmon resonance peak of Au32. The evolution of spectra with NP sizes clearly manifests the fact that the characteristic plasmon-resonance peak linewidth becomes narrower as the NP size increases.

Figure 5 displays the Kohn−Sham MOs and energy levels of the $Au17^-$ and Au32. It is found that $Au17^-$ has less degenerate and more molecular-like MO energy levels than Au32, which leads to broader plasmon line width. For the MOs near HOMO and LUMO, an apparent characteristic of valence orbitals is observed in $Au17^-$, whereas the contribution of d orbital increases considerably for Au32. For the lower energy occupied orbitals (up to the orbital 156 for $Au17^-$ and 297 for Au32), the electron densities are almost entirely located on the gold atoms. The density begins to distribute on the surface of gold NPs and even extend far beyond the NPs as the orbital energy levels increase. According to the degree of electron delocalization, they were divided into bulk, surface, and plasmon states.[62] The plasmon state density is mainly located in a vacuum and is often called the "nearly free electron-like" or "superatom" state;[63] its resonance with electronic field leads to a strong absorption band. As shown in Tables 1 and 2, the strongest absorption peaks of monomers are formed by electron transitions ranging from HOMO−24 to LUMO+8 for $Au17^-$ and from HOMO−14 to LUMO+8 for Au32 cluster. Therefore, the plasmon resonance peaks of $Au17^-$ and Au32 NPs mostly result from the plasmon oscillation.

C. NP Pairs. To understand how the NPs couple, we calculate the optical absorption spectra of $Au17^-$ pairs using TDDFT. The evaluation of absorption spectra of $Au17^-$ dimers as a function of the interparticle distance is shown in Figure 6. Here d denotes the distance between two nearest neighboring Au atoms of two NPs and is changed from 6.0 to 2.8 Å corresponding to the interparticle centroid distance of 1.15 to 0.83 nm. (2.8 Å is the Au atomic diameter and the dimer with d = 2.8 Å corresponds to two touched NPs.) For the dimers, we adopted the structures with highest symmetry.

As two NPs approach each other (the value of d decreases), the dimer's absorption bands arisen from the plasmon excitation red shift and the relative intensities of absorption bands increase dramatically. The alteration of MO energy levels with the interparticle separations gives a clue to the red-shift phenomena

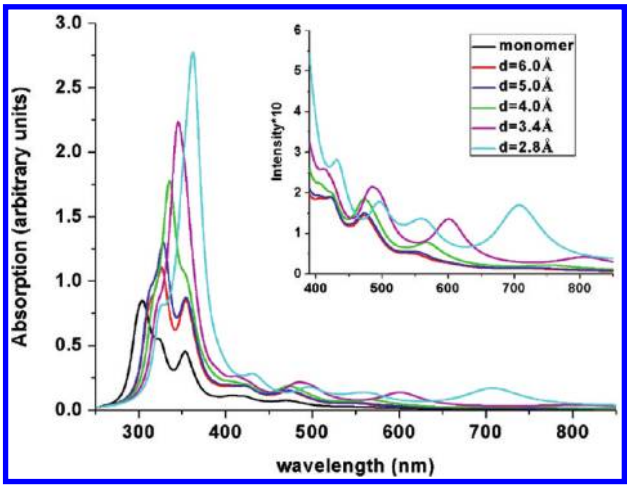

Figure 6. Calculated optical absorption spectra of $Au17^-$ dimers with different interparticle distances from 2.8 to 6 Å by TD-ωPBE. Spectral region varies from (a) 250 to 800 nm with normal intensity and (b) 350 to 800 nm with 10-fold intensity. The spectra were fitted using lorentz energy broadening of δ = 0.2 eV. The spectrum of isolated $Au17^-$ in solid line is shown for comparison.

of plasmon excitations because the excited states are formed by the electronic transitions from the occupied MOs to the virtual MOs. For $Au17^-$ dimers, as shown in Figure 7, the degenerate LUMOs have a tiny shift to low-lying energy level and the HOMO lowers more with increasing particle separation, leading to the increasing HOMO−LUMO gap as the interparticle separation increases. For Au32 nanopaticle dimers, the degenerate LUMOs move to upper level and the HOMOs shift to low-lying level with increasing separations, which also leads to the increasing HOMO−LUMO gap.

According to the changes of spectral lineshapes with reference to the spectrum of the isolated $Au17^-$, we divide the spectra of NP pairs into two categories. One has no explicit spectral line shape alteration but only an overall spectral red shift; another shows an apparent spectral red shift together with many additional new absorption bands in the low-energy range. Taking the dimer at d = 6.0 Å as an example, its overall spectrum red shifts compared to the monomer's spectrum. The strongest absorption band of this dimer is centered at 330 nm, red-shifted 30 nm

dx.doi.org/10.1021/jp2094092 |J. Phys. Chem. C 2012, 116, 1755–1763

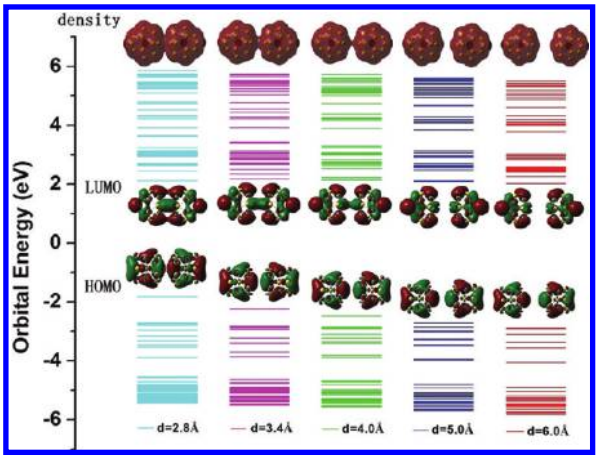

Figure 7. Molecular orbital energy levels and the spatial distribution of ground-state densities and frontier MOs of $Au17^-$ pairs with d = 2.8−6.0 Å.

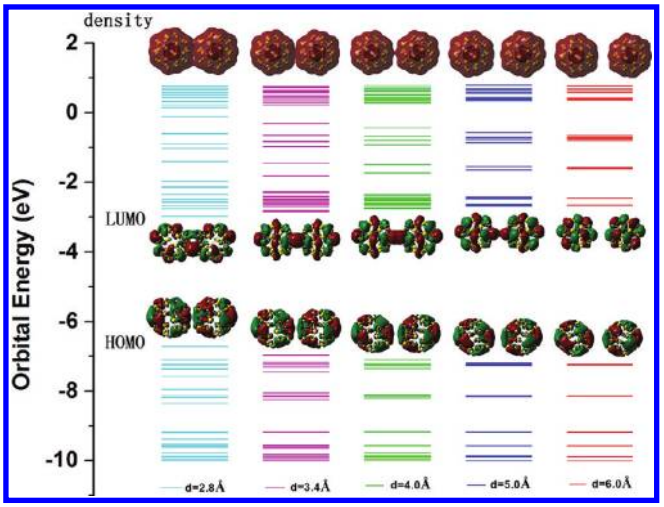

Figure 8. Molecular orbital energy levels and the spatial distribution of ground-state densities and frontier MOs of Au32 pairs with d = 2.8−6.0 Å.

compared with the corresponding monomer peak (centered at ∼300 nm), and its relative strength is less than twice that of the monomer. The spectral line shape alteration of this dimer can be well-explained by the mixed intramolecular Frenkel exciton and intermolecular charge-transfer exciton model. It is well known that when the MOs of the donor and the acceptor overlap, the intermolecular charge-transfer excitons (CTEs), for example, D^+A^-, D^-A^+, can be easily formed upon electronic excitation. There are four types of states of a single electron−hole pair: $|D^*A\rangle$, $|DA^*\rangle$, $|D^+A^-|\rangle$, and $|D^-A^+\rangle$. The first two states correspond to an electron and a hole on monomer "D" and on monomer "A" and can be created optically. The second pairs correspond to indirect electron−hole pairs, for example, electron on monomer "D" and hole on monomer "A" and are only created optically when two monomers couple. Two types of exciton states entangle to form new basis sets: $|FE^+\rangle = C_{11}|D^*A\rangle + C_{12}|DA^*\rangle$, $|FE^-\rangle = C_{21}|D^*A\rangle - C_{22}|DA^*\rangle$, $|CE^+\rangle = C_{33}|D^+A^-\rangle + C_{34}|D^-A^+\rangle$, and $|CE^-\rangle = C_{43}|D^+A^-\rangle - C_{44}|D^-A^+\rangle$. Then, the electron−hole pair Hamiltonian H in the above new basis sets can be constructed. The dimeric exciton states $|\Phi\rangle$ are obtained by solving the eigenvalue equation $H|\Phi\rangle = ES|\Phi\rangle$. If the excitation energies of FEs and CTEs are close, then the intramolecular and intermolecular excited states mix sufficiently to form mixed excited states of systems, which make the dimeric states possess the characters of both intramolecular and intermolecular excitations. The mixing degree between FEs and CTEs, the energy spacing, and the order of dark/bright exciton of dimer are determined by the excitation energies of FEs and CTEs and their coupling values as well.[61,64−66] Because of the contribution of dark intermolecular CT excitations to the excited states of the dimer, the intensity of the plasmon excitation is less than the twice that of the monomer.

As the two NPs approach each other further, such as the $Au17^-$ pairs with $d \leq 3.4$ Å and Au32 pairs with $d \leq 5.0$ Å, a pronounced red shift of the plasmon resonance band is shown and new excitation peaks appear. In this case, two NPs are strongly coupled, and there is significant overlap between the wave functions of the neighboring atoms. A bond-forming step takes place.[67] This is verified by the spatial distribution of LUMOs of $Au17^-$ and Au32 NP pairs. (See Figures 7 and 8.) However, we do not observe an apparent wave function overlap between HOMOs. The strength of the hybridization between the HOMOs is appreciably weaker than that between LUMOs because the occupied MOs are more localized than the unoccupied ones. The strong coupling between the unoccupied MOs is advantageous to electron transport between the NPs, which constitutes a channel through which charge can flow freely, leading to a large number of electrons populated in the junction of two NPs. (See the electron densities depicted

Table 3. Calculated Plasmonic Absorption Band of $Au17^-$ NP Dimers at Different Interparticle Distances

d	BSES	E (eV)	λ (nm)	f
6.0	S_{73}	3.4619	358.14	0.1748
	S_{78}	3.5027	353.97	0.3889
	S_{103}	3.7885	327.26	0.5265
	S_{119}	3.8916	318.59	0.1874
	S_{133}	3.9903	310.71	0.1602
	S_{136}	4.0071	309.41	0.2314
5.0	S_{73}	3.4450	359.90	0.1454
	S_{80}	3.5034	354.14	0.3704
	S_{105}	3.7697	328.89	0.7011
	S_{121}	3.8862	319.04	0.2047
	S_{137}	3.9758	311.85	0.2524
	S_{140}	4.0029	309.74	0.2166
4.0	S_{75}	3.4382	360.61	0.2056
	S_{80}	3.4946	354.79	0.3384
	S_{95}	3.6693	337.89	0.5882
	S_{101}	3.7016	334.95	0.6230
	S_{104}	3.7246	332.88	0.2061
	S_{129}	3.8865	319.01	0.1889
	S_{136}	3.9391	314.75	0.2351
3.4	S_{80}	3.4734	356.96	0.2822
	S_{87}	3.5136	352.87	0.5883
	S_{92}	3.6046	343.96	1.4715
	S_{129}	3.8672	320.60	0.3097
2.8	S_{79}	3.3951	365.18	0.1251
	S_{81}	3.4153	363.02	2.2026
	S_{134}	3.8279	323.90	0.3695

Table 4. Mulliken Population Analysis of the Ground and Singlet Excited States for $Au17^-$ Dimers at Different Interparticle Distances[a]

d	states	atom 6	atom 23	TC_1	TC_2
6.0	S_0	0.56	0.56	−1.0	−1.0
5.0	S_0	1.27	1.27	−1.0	−1.0
4.0	S_0	2.50	2.50	−1.0	−1.0
3.4	S_0	3.36	3.36	−1.0	−1.0
2.8	S_0	4.05	4.05	−1.0	−1.0
	S_6	4.07	4.07	−1.0	−1.0
	S_{79}	3.99	3.99	−1.0	−1.0
	S_{81}	3.98	3.98	−1.0	1.0

[a] Here only the electron populations located on two nearest neighboring Au atoms of monomers are shown (atom no. 6 and atom no. 23). The indices S_0, S_n, and TC_n denote the ground state, the nth singlet excited states, and the total charge of the nth NP, respectively.

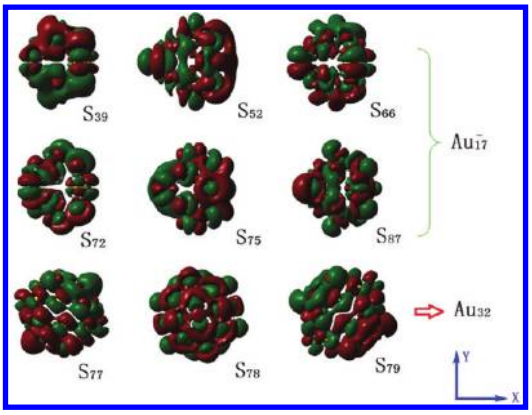

Figure 9. Transition densities of BSESs, which constitute the corresponding plasmon-resonance absorption band of isolated $Au17^-$ and Au32 clusters.

in Figures 7 and 8.) Additionally, there is a pronouncedly increased electron population in the nearest neighboring atoms with decreasing interparticle distance. (See Table 4.) The localized electrons can undoubtedly enhance the electromagnetic field in the gap of NP pairs, leading to the dramatically increased polarizability. The polarizability of the plasmon absorption band is even larger than twice that of the monomer. The increasing polarizability is explicitly originated from the two major factors: the reducing number of excited states contributed to the plasmon-resonance peaks (Table 3) and the increasing electrons localized in the gap as two NPs approach each other. It is explicit that the classical plasmon hybridization model or the exciton model fail to describe the optical responses of these closely spaced NPs and a full quantum mechanical description of the responses of NP pairs to light is inevitable. Qualitatively, our TDDFT computations for $Au17^-$ dimers provide optical properties that are in agreement with previously experimentally observed and theoretical trends for nanospheres.[28,30,68]

In Figures 9−11, we display the spatial distribution of transition densities for the corresponding BSESs, which construct the plasmon absorption bands of isolated NPs and NP pairs. For the isolated NPs, the induced dipoles of excited states are either parallel or perpendicular to the $x-y$ plane. For example, for Au32

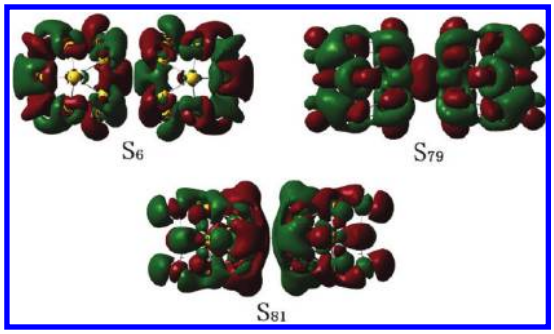

Figure 10. Transition densities of BSESs of nos. 6, 79, and 81, which constitute the plasmon-resonance absorption band of $Au17^-$ dimer at d = 2.8 Å.

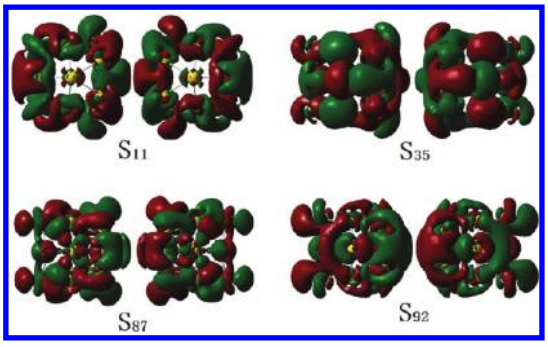

Figure 11. Transition densities of BSESs, which constitute the plasmon-resonance absorption band of $Au17^-$ dimer at d = 3.4 Å.

cluster, the induced dipoles in the 77 and 79th excited states are parallel to the plane, whereas that in the 78th is perpendicular to the $x-y$ plane. When two $Au17^-$ NPs approach each other, the dipoles of all bright excited states, except the 79th excited state in $Au17^-$ pair with d = 2.8 Å, are head-to-tail orientation, leading to the optically active, hybridized mode of the pair to be red-shifted from the single-dipole resonance frequency. However, the calculated Förster transfer coupling is much smaller than the interaction strength. For example, at d = 2.8 Å, the Frenkel exciton couplings are in the range of 0.01 to 0.03 eV. Those small exciton coupling values cannot red shift the plasmon resonance peaks as dramatically as Figure 6 shows. Instead, the strong hybridization between the MOs in an NP pair induces the charges to redistribute compared with the isolated NP, which enhances electromagnetic field around NPs and further red shifts the spectra.

IV. CONCLUSIONS

On the basis of DFT and TDDFT, we have studied the electronic structures and optical properties of isolated small-size Au NPs with different sizes and coupled NP pairs with different interparticle distances. The following conclusions have been drawn from this research work.

(1) The TD-LRC-DFT gives a more reasonable description of the electron excitation of Au NPs than the conventional functionals, such as PBE. It correctly yields the apparent plasmonic characteristics of Au NPs and places most of the absorption intensity near the absorption maximum, whereas the oscillator strength yielded by PBE functional spreads among more transitions, leading to an overall decrease in the absorption intensity.

dx.doi.org/10.1021/jp2094092 |J. Phys. Chem. C 2012, 116, 1755–1763

(2) The plasmon resonance of isolated NPs is sensitive to NP sizes. The absorption band resulted from the plasmon excitation red shifts with the increasing NP sizes, in agreement with the experimentally observed trends of the spectral shift. For example, the strongest optical absorption peak blue shifts from 357 to 305 nm when the number of Au atoms in NP is reduced from 32 to 17. The line width of characteristic plasmon-resonance peaks becomes wider with the decreasing NP sizes, reflecting deviations of the material response from that of the bulk metals.

(3) When two separated metal NPs are brought together, a significant interparticle interaction and thus its impact on excited states of a NP pair can be seen. The wavelength shift resulting from this interparticle coupling sensitively depends on the particle separation, providing a clear signature for sensing applications.

(4) When the complex structures interact weakly, their optical responses can often be explained in terms of the coupling of localized excitations in individual components of the structure. The exciton coupling model or the excimer theory is usually used to describe the interaction between two chromophores and its impact on the excited states. The electronically excited states of a dimer are related to the excited states of the monomer. However, for the closely spaced NPs, the calculated coupling values of localized excitations (Frenkel exciton couplings) are too small to red shift dramatically the plasmon resonance peaks of a NP pair. The localized exciton coupling model fails to describe the spectra of closely spaced NPs. Other interparticle interactions, such as the charge polarization effect and electron exchange interactions, play a significant role in the properties of a closely spaced NP pair, which are even larger than those in organic molecular dimers with similar molecular orientation and intermolecular distance.[61,64−66]

(5) As two NPs approach near touching contact, for example, the $Au17^{-}$ pairs with $d \leq 3.4$ Å and Au32 pairs with $d \leq 5.0$ Å, two NPs are strongly coupled and there is significant overlap between the wave functions of two individual NPs. A bond-forming step takes place. The strong coupling between the unoccupied MOs is advantageous to electron transport between the NPs. Therefore, the electrons in a closely spaced NP pair redistribute to reach a optimal charge distribution compared with the NPs without the interparticle interaction or weak interaction. We observe that a large number of electrons are populated in the gap and in the nearest neighboring atoms of two NPs. The localized electrons can undoubtedly enhance the electromagnetic field in the gap of two NP. As a result, a pronounced red shift of the plasmon-resonance band with decreasing interparticle distance is shown, and many new absorption peaks appear in the low-energy range.

AUTHOR INFORMATION

Corresponding Author

*E-mail: liangwz@ustc.edu.cn.

ACKNOWLEDGMENT

Financial supports from National Science Foundation of China (grant no. 20833003 and no. 21073168), the National Basic Research Program of China (grant no. 2011CB808501) are acknowledged.

REFERENCES

(1) El-Sayed, M. A. *Acc. Chem. Res.* **2001**, *34*, 257–264.
(2) Haes, A. J.; Zou, S. L.; Schatz, G. C.; Van Duyne, R. P. *J. Phys. Chem. B* **2004**, *108*, 6961–6968.
(3) Danckwerts, M.; Novotny, L. *Phys. Rev. Lett.* **2007**, *98*, 026104.
(4) Fofang, N. T.; Park, T.-H.; Neumann, O.; Mirin, N. A.; Nordlander, P.; Halas, N. J. *Nano Lett.* **2008**, *8*, 3481–3487.
(5) Lassiter, J. B.; Sobhani, H.; Fan, J. A.; Kundu, J.; Capasso, F.; Nordlander, P.; Halas, N. J. *Nano Lett.* **2010**, *10*, 3184–3189.
(6) Pelton, J.; Aizpurua, M; Bryant, G. *Laser Photonics Rev.* **2008**, *2*, 136–159.
(7) Shegai, T.; Li, Z.; Dadosh, T.; Zhang, Z.; Xu, H.; Haran, G. *Proc. Natl. Acad. Sci. U.S.A.* **2008**, *105*, 16448C16453.
(8) Link, S.; El-Sayed, M. A. *J. Phys. Chem. B* **1999**, *103*, 8410–8426.
(9) Alvarez, M. M.; Khoury, J. T.; Schaaff, T. G.; Shafigullin, M. N.; Vezmar, I.; Whetten, R. L. *J. Phys. Chem. B* **1997**, *101*, 3706–3712.
(10) Kelly, K. L.; Coronado, E.; Zhao, L. L.; Schatz, G. C. *J. Phys. Chem. B* **2003**, *107*, 668–677.
(11) Sun, Y.; Xia, Y. *Science* **2002**, *298*, 2176–2179.
(12) Sherry, L. J.; Chang, S.-H.; Schatz, G. C.; Duyne, R. P. V; Wiley, B. J.; Xia, Y. *Nano Lett.* **2005**, *5*, 2034–2038.
(13) Nehl, C. L.; Liao, H.; Hafner, J. H. *Nano Lett.* **2006**, *6*, 683–688.
(14) Mie, G. *Ann. Phys.* **1908**, *25*, 377–445.
(15) Miller, E. K. *J. Electromagn. Waves Appl.* **1994**, *8*, 1125–1172.
(16) Purcell, E. M.; Pennypacker, C. R. *Astrophys. J.* **1973**, *186*, 705–714.
(17) Draine, B. T.; Flatau, P. J. *J. Opt. Soc. Am. A* **1994**, *11*, 1491–1499.
(18) Hafner, C. H.; Ballist, R. *Int. J. Comput. Electr. Electron. Eng.* **1983**, *2*, 1.
(19) Pendry, J. B.; MacKinnon, A. *Phys. Rev. Lett.* **1992**, *69*, 2772–2775.
(20) Jin, J. *The Finite Element Method in Electromagnetics*, 2nd ed.; Wiley: New York, 2002.
(21) Zhao, J.; Pinchuk, A.; Mcmahon, J. M.; Li, S.; Ausman, L. K.; Atkinson, A. L.; Schatz, G. C. *Acc. Chem. Res.* **2008**, *41*, 1710–1720.
(22) Morton, S. M.; Silverstein, D. W.; Jensen, L. *Chem. Rev.* **2011**, *111*, 3962.
(23) Li, J. F.; Huang, Y. F.; Ding, Y.; Yang, Z. L.; Li, S. B.; Zhou, X. S.; Fan, F. R.; Zhang, W.; Zhou, Z. Y.; Wu, D. Y.; Ren, B.; Wang, Z. L.; Tian, Z. Q. *Nature* **2010**, *464*, 392–395 .
(24) Halas, N. J.; Lal, S.; Chang, W. S.; Link, S.; Nordlander, P. *Chem. Rev.* **2011**, *111*, 3913–3961.
(25) Prodan, E.; Radloff, C.; Halas, N. J.; Nordlander, P. *Science* **2003**, *302*, 419–422.
(26) Jain, P. K.; Huang, W.; El-Sayed, M. A. *Nano Lett.* **2007**, *7*, 2080–2088.
(27) Wang, H.; Brandl, D.; Nordlander, P.; Halas, N. *Acc. Chem. Res.* **2007**, *40*, 53–62.
(28) Nordlander, P.; Oubre, C.; Prodan, E.; Li, K.; Stockman, M. I. *Nano Lett.* **2004**, *4*, 899–903.
(29) Sheikholeslami, S.; Jun, Y.-W.; Jain, P. K.; Alivisatos, A. P. *Nano Lett.* **2010**, *10*, 2655–2660.
(30) Atay, T.; Song, J. H.; Nurmikko, A. V. *Nano Lett.* **2004**, *4*, 1627–1631.
(31) Aizpurua, J.; Bryant, G. W.; Richter, L. J.; García de Abajo, F. J.; Kelly, B. K.; Mallouk, T. *Phys. Rev. B* **2005**, *71*, 235420.
(32) Romero, I.; Aizpurua, J.; Bryant, G. W.; García de Abajo, F. J. *Opt. Express* **2006**, *14*, 9988–9999.
(33) Gersten, J. I.; Nitzan, A. *Surf. Sci.* **1985**, *158*, 165–189.
(34) Schmeits, M.; Dambly, L. *Phys. Rev. B* **1991**, *44*, 12706.
(35) Tamaru, H.; Kuwata, H.; Miyazaki, H. T.; Miyano, K. *Appl. Phys. Lett.* **2002**, *14*, 348–350.
(36) Rechberger, W.; Hohenau, A.; Leitner, A.; Krenn, J. R.; Lamprecht, B.; Aussenegg, F. *Opt. Commun.* **2003**, *220*, 137–141.
(37) Su, K. -H.; Wei, Q. -H.; Zhang, X.; Mock, J. J.; Smith, D. R.; Schultz, S. *Nano Lett.* **2003**, *3*, 1087–1090.

(38) Futamata, M.; Maruyama, Y.; Ishikawa, M. *J. Phys. Chem. B* **2003**, *107*, 7607–7617.
(39) Prikulis, J.; Svedberg, F.; Kall, M.; Enger, J.; Ramser, K.; Goksor, M.; Hanstorp, D. *Nano Lett.* **2004**, *4*, 115–118.
(40) Ghosh, S. K.; Pal, T. *Chem. Rev.* **2007**, *107*, 4787.
(41) Kim, D. S.; Heo, J.; Ahn, S. H.; Han, S. W.; Yun, W. S.; Kim, Z. H. *Nano Lett.* **2009**, *9*, 3619–3625.
(42) Sardar, R.; Funston, A. M.; Mulvaney, P.; Murray, R. W. *Langmuir* **2009**, *25*, 13840–13851.
(43) Cooper, G. M.; Hausman, R. E. *The Cell: A Molecular Approach*; ASM Press: Washington, DC, 2008; p 361.
(44) Häkkinen, H.; Yoon, B.; Landman, U.; Li, X.; Zhai, H.-J.; Wang, L.-S. *J. Phys. Chem. A* **2003**, *107*, 6168–6175.
(45) Johansson, M. P.; Lechtken, A.; Schooss, D.; Kappes, M. M.; Furche, F. *Phys. Rev. A* **2008**, *77*, 053202.
(46) Bulusu, S.; Li, X.; Wang, L.-S.; Zeng, X. C. *Proc. Natl. Acad. Sci. U.S.A.* **2006**, *103*, 8326–8330.
(47) Huang, W.; Bulusu, S.; Pal, R.; Zeng, X. C.; Wang, L. S. *ACS Nano* **2009**, *3*, 1225–1230.
(48) Xing, X. P.; Yoon, B.; Landman, U.; Parks, J. H. *Phys. Rev. B* **2006**, *74*, 165423.
(49) Ji, M.; Gu, X.; Li, X.; Gong, X. G.; Li, J.; Wang, L. S. *Angew. Chem., Int. Ed.* **2005**, *44*, 7119–7123.
(50) Johansson, M. P.; Sundholm, D.; Vaara, J. *Angew. Chem., Int. Ed.* **2004**, *43*, 2678–2681.
(51) Fa, W.; Zhou, J.; Luo, C. F.; Dong, J. M. *Phys. Rev. B* **2006**, *73*, 085405.
(52) Jalbout, A. F.; Contreras-Torres, F. F.; Pérez, L. A.; Garzón, I. L. *J. Phys. Chem. A* **2008**, *112*, 353–357.
(53) Frisch, M. J.; Trucks, G. W.; Schlegel, H. B.; Scuseria, G. E.; Robb, M. A.; Cheeseman, J. R.; Montgomery, J. A., Jr.; Vreven, T.; Kudin, K. N.; Burant, J. C.; Millam, J. M.; Iyengar, S. S.; Tomasi, J.; Barone, V.; Mennucci, B.; Cossi, M.; Scalmani, G.; Rega, N.; Petersson, G. A.; Nakatsuji, H.; Hada, M.; Ehara, M.; Toyota, K.; Fukuda, R.; Hasegawa, J.; Ishida, M.; Nakajima, T.; Honda, Y.; Kitao, O.; Nakai, H.; Klene, M.; Li, X.; Knox, J. E.; Hratchian, H. P.; Cross, J. B.; Bakken, V.; Adamo, C.; Jaramillo, J.; Gomperts, R.; Stratmann, R. E.; Yazyev, O.; Austin, A. J.; Cammi, R.; Pomelli, C.; Ochterski, J. W.; Ayala, P. Y.; Morokuma, K.; Voth, G. A.; Salvador, P.; Dannenberg, J. J.; Zakrzewski, V. G.; Dapprich, S.; Daniels, A. D.; Strain, M. C.; Farkas, O.; Malick, D. K.; Rabuck, A. D.; Raghavachari, K.; Foresman, J. B.; Ortiz, J. V.; Cui, Q.; Baboul, A. G.; Clifford, S.; Cioslowski, J.; Stefanov, B. B.; Liu, G.; Liashenko, A.; Piskorz, P.; Komaromi, I.; Martin, R. L.; Fox, D. J.; Keith, T.; Al-Laham, M. A.; Peng, C. Y.; Nanayakkara, A.; Challacombe, M.; Gill, P. M. W.; Johnson, B.; Chen, W.; Wong, M. W.; Gonzalez, C.; Pople, J. A. *Gaussian 03*, revision D.01; Gaussian, Inc.: Wallingford, CT, 2004.
(54) Gilb, S.; Jacobsen, K.; Schooss, D.; Furche, F.; Ahlrichs, R.; Kappesb, M. M. *J. Chem. Phys.* **2004**, *121*, 4619–4627.
(55) Chai, J.-D.; Head-Gordon, M. *J. Chem. Phys.* **2008**, *128*, 084106.
(56) Rohrdanz, M. A.; Martins, K. M.; Herberta, J. M. *J. Chem. Phys.* **2009**, *130*, 054112.
(57) Perdew, J. P.; Burke, K.; Ernzerhof, M. *Phys. Rev. Lett.* **1996**, *77*, 3865–3688.
(58) Adamo, C.; Barone, V. *Chem. Phys. Lett.* **1998**, *298*, 113–119.
(59) Chai, J.-D.; Head-Gordon, M. *Chem. Phys. Lett.* **2008**, *467*, 176–178.
(60) Shao, Y.; Molnar, L. F.; Jung, Y.; Kussmann, J.; Ochsenfeld, C.; Brown, S. T.; Gilbert, A. T. B.; Slipchenko, L. V.; Levchenko, S. V.; O'Neill, D. P.; DiStasio, R. A.; Lochan, R. C.; Wang, T.; Beran, G. J. O.; Besley, N. A.; Herbert, J. M.; Lin, C. Y.; Van Voorhis, T.; Chien, S. H.; Sodt, A.; Steele, R. P.; Rassolov, V. A.; Maslen, P. E.; Korambath, P. P.; Adamson, R. D.; Austin, B.; Baker, J.; Byrd, E. F. C.; Dachsel, H.; Doerksen, R. J.; Dreuw, A.; Dunietz, B. D.; Dutoi, A. D.; Furlani, T. R.; Gwaltney, S. R.; Heyden, A.; Hirata, S.; Hsu, C. P.; Kedziora, G.; Khalliulin, R. Z.; Klunzinger, P.; Lee, A. M.; Lee, M. S.; Liang, W.; Lotan, I.; Nair, N.; Peters, B.; Proynov, E. I.; Pieniazek, P. A.; Rhee, Y. M.; Ritchie, J.; Rosta, E.; Sherrill, C. D.; Simmonett, A. C.; Subotnik, J. E.; Woodcock, H. L.; Zhang, W.; Bell, A. T.; Chakraborty, A. K.; Chipman, D. M.; Keil, F. J.; Warshel, A.; Hehre, W. J.; Schaefer, H. F.; Kong, J.; Krylov, A. I.; Gill, P. M. W.; Head-Gordon, M. *Phys. Chem. Chem. Phys.* **2006**, *8*, 3172.
(61) Song, J.; Gao, F.; Shi, B.; Liang, W. Z. *Phys. Chem. Chem. Phys.* **2010**, *12*, 13070–13075.
(62) Guo, Z. Y.; Habenicht, B. F.; Liang, W. Z.; Prezhdo, O. V. *Phys. Rev. B* **2010**, *81*, 125415.
(63) Zhao, J.; Feng, M.; Yang, J.; Petek, H. *ACS Nano* **2009**, *3*, 853–864.
(64) Pan, F.; Gao, F.; Liang, W. Z. *J. Phys. Chem. B* **2009**, *113*, 14581–14587.
(65) Gao, F.; Zhao, Y.; Liang, W. Z. *J. Phys. Chem. B* **2011**, *115*, 2699–2708.
(66) Gao, F.; Liang, W. Z.; Zhao, Y. *Sci. China: Chem.* **2010**, *53*, 297–309.
(67) Troparevsky, M. C.; Zhao, K.; Xiao, D.; Eguiluz, A. G.; Zhang, Z. Y. *Phys. Rev. B* **2008**, *82*, 045413.
(68) Olk, P.; Renger, J.; Wenzel, M. T.; Eng, L. M. *Nano Lett.* **2008**, *8*, 1174–1178.